ASEG-PESA 2013
'THE EUREKA MOMENT'
11-14 AUGUST 2013 • MELBOURNE, AUSTRALIA

Large-scale magnetic inversion using differential equations and ocTrees

Kristofer Davis
UBC-Geophysical Inversion Facility
Dept. of Earth and Ocean Sciences
University of British Columbia
2207 Main Mall
Vancouver, BC V6T 1Z4 Canada
kdavis@eos.ubc.ca

Eldad Haber
UBC-Geophysical Inversion Facility
Dept. of Earth and Ocean Sciences
University of British Columbia
2207 Main Mall
Vancouver, BC V6T 1Z4 Canada
haber@math.ubc.ca

Doug Oldenburg
UBC-Geophysical Inversion Facility
Dept. of Earth and Ocean Sciences
University of British Columbia
2207 Main Mall
Vancouver, BC V6T 1Z4 Canada
doug@eos.ubc.ca

SUMMARY

The inversion of large-scale magnetic data sets has historically been successfully achieved through integral transforms of the large, dense sensitivity matrix. Two well-known transforms, the discrete Fourier and multi-dimensional wavelet, reduce the required storage and ultimately speed of the inversion by storing only the necessary transform coefficients without losing accuracy. The main drawback of the approaches is the required calculation of the entire dense sensitivity matrix prior to the transform. This process can be much more costly than the inversion itself. We solve the magnetostatic Maxwell's equation using a finite volume technique on an ocTree-based mesh. The ocTree mesh greatly reduces the time required for the inversion process. When working in the differential equation domain it is not necessary to explicitly form the sensitivity matrix; this decreases the storage requirement of the problem and increases the overall speed of the inversion. The principal mesh is broken up into sub-domain ocTree grids to further enable parallelization of the forward problem. These grids extend the entire domain of the principal mesh to include large regional features that may influence the data. We present the discretization of the equations and verify the accuracy of the modelling both with the principal mesh and with multiple sub-domains. We show a synthetic example and a large field example consisting of over 4 million data and 5 million model cells that was inverted on a desktop computer.

Key words: Inversion, magnetostatic Maxwell's equations, large-scale, potential fields

INTRODUCTION

Airborne magnetic surveys often acquire tens of thousands to hundreds of thousands of data. It is desirable to invert these data to recover a three-dimensional distribution of susceptibility. High-resolution models can be used as an exploration tool by examining the recovered physical parameters rather than transforms of the observed field. Unfortunately, the combination of numerous observations and the discretization of the subsurface can lead to an inversion that is intractable. Numerous methods have been developed in order to reduce inversion time or physical memory required for the inversion of magnetic data. These have primarily been in the realm of the transforming and storing the dense matrix of sensitivities through integral transforms. For example, the discrete Fourier transform (DFT) has been used successfully in inversion (Mareschal, 1985; Cordell, 1992; Pilkington, 1997) and is quite fast. However, it has drawbacks such as requiring evenly gridded data located on a horizontally flat plane. Li and Oldenburg (2003, 2010) employed multi-dimensional wavelet transforms to represent the dense sensitivity matrix sparsely. The main challenge of this approach is that the complete matrix must be calculated prior to the transform. Although this can be done on a row-by-row basis to save physical memory on a computer, the time required can still be much longer than the actual inversion itself.

We choose to solve the common elliptic div-grad equation derived from Maxwell's equations for magnetostatics. The approach is similar to that of Lelièvre and Oldenburg (2006) in which they solved for high susceptibilities. The problem size is decreased through the use of an ocTree mesh (e.g. Ascher and Haber, 2001; Haber *et al.*, 2007) to decrease model parameters. Further decomposition of the large ocTree domain into smaller ocTree meshes allows the forward modelling to be parallelized. Each domain contains small cells near observation locations that transition into large cells covering the remaining limits of the main ocTree mesh. These large cells recover regional features away from the locations where high resolution is unnecessary. Another principal benefit arises from not explicitly forming the dense matrix that is required through the integral equation approach. This can save a significant amount of time over the entire inversion process. Lastly, the amount of data does not directly affect the size of the inversion as the fields are solved on the model and then interpolated to the observations.

In this paper we briefly discuss the governing equations and finite volume discretization method as it applies to the ocTree discretization. Accuracies of the forward modelling are presented as well as the general inversion methodology. A discussion on domain decomposition is given and synthetic and field examples are presented.

FORWARD MODELLING

Maxwell's equations for a static magnetic field with no sources are:

$$\nabla \times \mathbf{H} = \nabla \times \mathbf{M} \quad \mathbf{H} \in \Omega \tag{1a}$$
$$\nabla \cdot \mu \mathbf{H} = 0 \quad \mathbf{H} \in \Omega \tag{1b}$$
$$\mathbf{n} \times \mathbf{H} = \mathbf{n} \times \mathbf{H}_0 \quad \mathbf{H} \in \partial\Omega \tag{1c}$$
$$\mathbf{n} \cdot \mathbf{H} = \mathbf{n} \cdot \mathbf{H}_0 \quad \mathbf{H} \in \partial\Omega \tag{1d}$$

where **H** is the magnetic field, μ is the magnetic permeability, and **M** are magnetic sources. We first assume that there are no magnetic sources, **M** = 0. It follows that

$$\nabla \cdot \mu \mathbf{H} = 0 \tag{2}$$

and we also assume that

$$\mu = \mu_o(1 + \chi) \tag{3}$$

where $\mu_o = 4\pi \times 10^{-7}$ is the permeability of free space, χ is the magnetic susceptibility and is small ($0 \leq \chi \ll 1$). The primary/secondary approach is then employed, letting $\mathbf{H} = \mathbf{H}_o + \mathbf{H}_s$ where $\mathbf{H}_o$ is the earth's magnetic field (i.e. the field with χ = 0). Then the linearization of equations 1a – 1d yield

$$\nabla \times \mathbf{H}_s = 0 \quad \mathbf{H}_s \in \Omega \tag{4a}$$
$$\nabla \cdot \mu_o \mathbf{H}_s = -\mu_o \nabla \cdot \chi \mathbf{H}_o \quad \mathbf{H}_s \in \Omega \tag{4b}$$
$$\mathbf{n} \times \mathbf{H}_s = 0 \quad \mathbf{H}_s \in \partial\Omega \tag{4c}$$
$$\mathbf{n} \cdot \mathbf{H}_s = 0 \quad \mathbf{H}_s \in \partial\Omega \tag{4d}$$

It should be noted that one could relax the small magnetic permeability assumption and solve a non-linear set of equations that would take into account the effect of self-demagnetization. In this paper, however, the Born approximation has been used to disregard the coupling between the anomalous field and the anomaly and assume purely induced magnetization. It follows from equation 4a that $\mathbf{H}_s = -\nabla\phi$ and this leads to the Poisson equation for the potential ϕ:

$$\nabla^2\phi = \nabla \cdot \chi \mathbf{H}_s$$
$$\hat{n} \times \nabla\phi = 0 \quad \text{on } \partial\Omega \tag{5}$$

that can be solved using a finite-volume method when discretised on a tensor mesh. One important aspect of the finite volume discretization is the level of accuracy that is dependent upon the cell size and average permeability values. Once on a small enough grid, the set of equations can then be accurately expanded to $\mathbf{D}\mu_o\mathbf{H}_s = -\mu_o\mathbf{D}\mathbf{X}\mathbf{H}_o$ so that **G**, is the gradient operator, **D** is the divergence operator, and **X** are the harmonically averaged discrete susceptibilities. Rather than completely form the sensitivities, we choose to solve for the data $\mathbf{H}_s = -\mu_o\mathbf{D}\mathbf{H}_o\mathbf{G}[(\mathbf{D}\mu_o\mathbf{G})^{-1}\mathbf{X}]$. Given the discrete values of χ and the measurements of $\mathbf{H}_o$ and $\mathbf{H}_s$, the general forward modelling scheme takes the symbolic form of

$$\mathbf{d} = \mathbf{J}\chi \tag{6}$$

where the sensitivities, **J**, are calculated on a mesh. However, it should be noted that **J** is never explicitly formed. The problem of $(\mathbf{D}\mu_o\mathbf{G})^{-1}\mathbf{X}$ is solved via projected-conjugate gradients (Vogel, 2002) each time the sensitivity multiplied by a vector is required. Only the discrete operators need to be stored.

Working with small cells to retain accuracy can lead to excessively large problems. We use a semi-structured mesh to handle such problems. An ocTree-based discretization is utilized to create small cells where accuracy is more important and coarser cells elsewhere. This decreases the amount of storage required for the modelling and inversion. Furthermore, the mesh volume should be continued far from the observation locations to account for the zero boundary conditions imposed in equation 5. An added benefit in utilizing an ocTree mesh is that it accommodates this assumption yet minimizes the number of required model parameters.

OCTREE DISCRETIZATION

OcTree discretization is an approach that creates a semi-structured grid in order to preserve accuracy yet decrease the amount of computation storage required. For linear problems, ocTrees are determined prior to calculating the kernel functionals because the forward modelling requires only matrix-vector operations. Adaptive discretization can significantly reduce the storage requirement for non-linear methods through multi-grid methods (e.g. Haber *et al.*, 2007).

OcTrees are based on a hierarchical structure and require the finest possible mesh to be dimensions of $2^I \times 2^J \times 2^K$. The mesh begins coarse, splitting cells into quadrants to increase resolution as necessary. This process of local grid refinement can be done on multiple grids and then combined to create the final mesh. We choose this hybrid approach by applying an ocTree discretization based on prior information, such as topography, geology, and survey design. The mesh is regularized so that each cell either has one or two neighbours for every direction. The finest cell size is discretised around each observation location either in a sphere for borehole data or a hemisphere for surface and airborne data. The radius of the sphere or hemisphere is given by the user. This step is repeated once more at the next finest cell size for another radius. A typical value of the radius of the inner sphere is line spacing. An illustration of an ocTree mesh (used in the synthetic example) is shown in Figure 1. Dark blue cells represent single cells of $1 \times 1 \times 1$ and red largest cell size $(16 \times 16 \times 16)$. Data locations are shown as white dots.

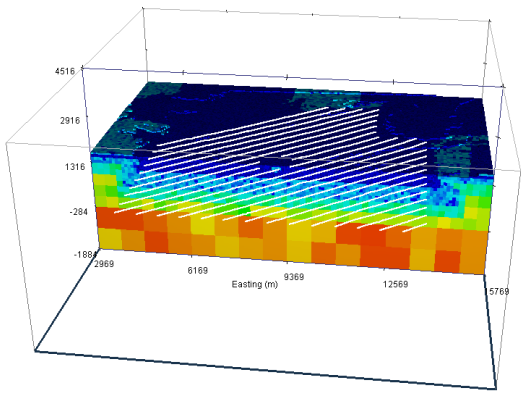

Figure 1: OcTree discretization of a dataset. The darker colours represent the finest cell size.

VERIFICATION OF FORWARD MODELLING

We examine the accuracy of the forward modelling approach by calculating the response 50-m^3 block with an SI=0.01 down an intersecting, vertical borehole. Data were modelled 1000 m above to 1000 m below the block every 50 m. The respective inclination, declination, and field strength for the study was 90˚, 0˚, and 60,000 nT. The integral equation from Bhattacharyya (1964) is used as a benchmark and the differential solution is calculated with four varying cell sizes on an ocTree mesh: 6.25 m, 12.5 m, 25 m, and 50 m. The left panel of Figure 2 shows the modelled data. The difference as a function of percentage, based on the integral solution, is presented on the middle panel. The total difference in nT is displayed on the right panel. The largest percentage differences for the 12.5-m and 6.25-m models near the block were 3.1% and 0.95%, respectively. The maximum signal difference of these cell sizes were respectively 0.38 and 0.15

nT. This panel shows that the cell size required for highly accurate results should be at least four times smaller than the body. The percentage increases far away from the block due to the small amplitude of the signals used in the comparison.

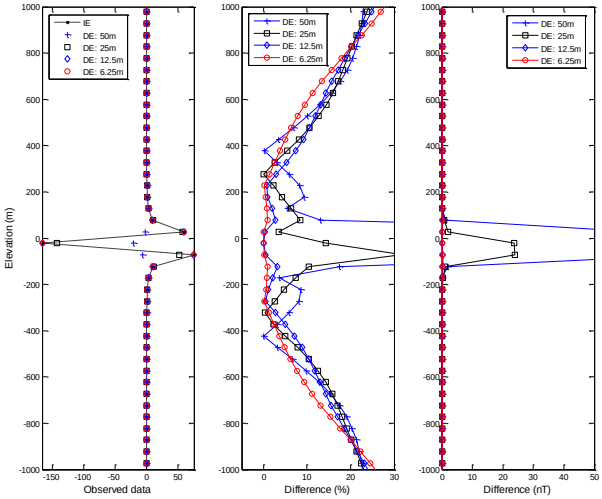

Figure 2: (left) The modelled responses of a 50m^3 block with the integral equation and differential equations. Cell sizes range from 6.25 m to 50 m for the differential calculation. The differences are shown in terms of percentage (centre) compared to the integral solution. The right-hand plot shows the absolute difference in nT.

DOMAIN DECOMPOSITION

An increase in speed for the forward modelling algorithm can be achieved by dividing the ocTree mesh into multiple smaller domains. The domains are also ocTrees and contain small cells in their primary areas and then expand to large cells to cover the entire mesh region. In Figure 3, a slice of a sub-domain (right) and its main volume (left) are shown. The data locations are in white. The data locations used for the forward calculation by the sub-domain are also shown.

The forward modelling can then be performed over *p* domains by

$$\mathbf{d}^{\text{pre}} = \sum_{i=1}^{p} \mathbf{Q}\mathbf{J}(\mathbf{P}_i\chi) \tag{7}$$

where **Q** is the interpolation matrix from the ocTree mesh to the data, and $\mathbf{P}_i$ is an interpolation matrix from volumes in the i^{th} sub-domain to the corresponding volumes in the main mesh. Therefore, the forward problem is calculated on each sub-domain, but the susceptibilities are located on the principal mesh for regularization within the inverse problem. This is the topic of the next section.

INVERSION METHODOLOGY

The inversion of an adaptive ocTree-based model mesh is straightforward once the neighbouring cells are established. The discretised earth contains *m* rectangular prisms each having a constant susceptibility, χ. The inverse problem is solved using a traditional Gauss-Newton strategy of $\min \phi = \phi_d + \beta\phi_m$ where ϕ_d is the data misfit, ϕ_m is the

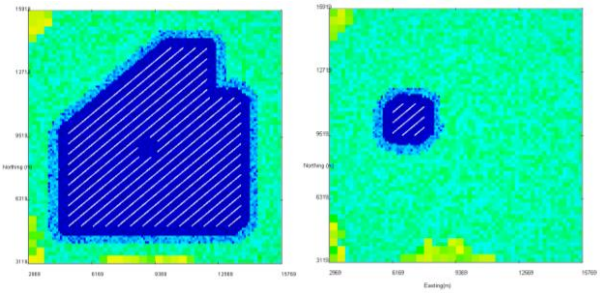

Figure 3: (left) The principal ocTree mesh that is broken into sub-domains for fast forward modelling. (right) An example of a sub-domain. The data locations are shown in white. Darker colours correlate to smaller cell sizes.

objective function, and β is a positive weighting parameter. The data misfit function quantifies how well the forward problem reproduces the observed data. The forward problem is parallelized over *p* sub-domains so that the data misfit is

$$\phi_d = \left\| \mathbf{W}_d \left[\sum_{i=1}^{p} \mathbf{Q}\mathbf{J}(\mathbf{P}_i\chi) - \mathbf{d} \right] \right\|_2^2 \tag{8}$$

where **Q**, **J**, and **P** are consistent with equation 7, **d** is the observed data, and $\mathbf{W}_d$ is a diagonal matrix containing the inverse standard deviations of each datum. The model objective function quantifies the model smoothness through the derivatives of the model and can incorporate a reference model, χ_o, if desired. The model objective function is calculated based on the values of the susceptibility throughout the entire principal ocTree mesh and is given by

$$\phi_m = \|\mathbf{W}_m(\chi - \chi_o)\|_2^2 \tag{9}$$

A sensitivity-based weighting is applied implicitly into $\mathbf{W}_m$ to offset the natural decay of the kernel function (Li and Oldenburg, 2000). Positivity is required for the susceptibilities. We choose to use a projected-gradient approach for the solution of $\Delta\mathbf{m}$ during the Gauss-Newton iterations.

SYNTHETIC EXAMPLE

Synthetic data were produced by three anomalies along 200-m spaced lines at a 30˚ angle from north. The 10,593 data (top left of Figure 5) were calculated using the integral equation approach at an inclination of 73˚, a declination of 18˚, and a field strength of 54,780 nT. A model mesh containing 50-m cells was used for the inversion for both the integral and differential equation approaches. The integral approach used 813,742 cells and a slice of the recovered model at 800 m of depth is shown on the bottom right of Figure 5. The ocTree approach required 230,710 cells and a slice of the mesh itself can be seen in Figure 3 (left). The inverted model is shown at the same depth on the lower left panel of Figure 5.

FIELD EXAMPLE

The field example comes from an airborne magnetics survey acquired in five blocks in northern British Columbia, Canada

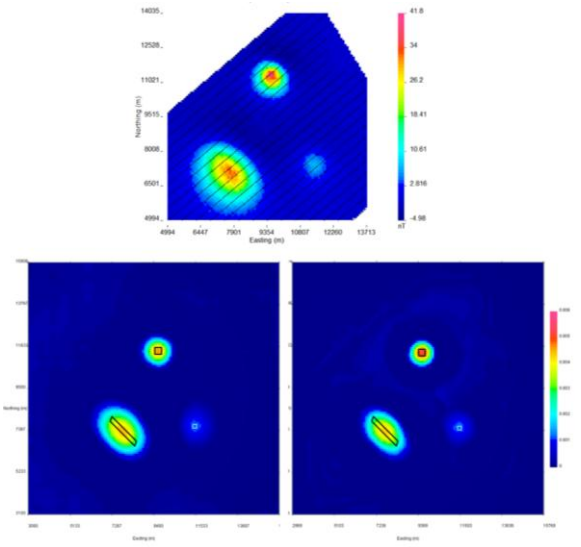

Figure 5: (top) The observed data. (bottom right) An inversion using the integral equation technique. (bottom left) An inversion using differential equations on an ocTree mesh.

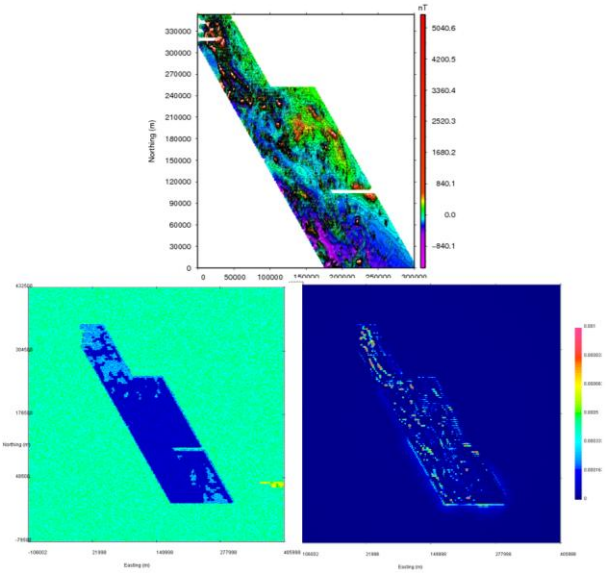

Figure 6: (top) The observed data. (bottom left) A slice through the principal mesh. (bottom right) A preliminary recovered model from the inversion.

acquired for Geoscience BC. The 4,031,671 data are shown at the top of Figure 6 and cover an area of more than 15,000 km^2. The ocTree mesh used for the inversion contained 5,644,591 cells with the smallest dimensions of 500 x 500 x 250 m, consistent with a reported inversion that required more than 20 tiles using the integral equation method (Phillips *et al.* 2009). A depth slice of the ocTree mesh is given on the bottom left of Figure 6. A preliminary recovered model from the inversion is located on the bottom right. The algorithm required less than 20 Gb of memory enabling it to be run on a desktop computer in the matter of a few hours. Specifics of the inversion will be discussed during the presentation.

CONCLUSIONS

We use a differential equation formulation to invert magnetic data on semi-structured ocTree meshes. The ocTree mesh is based upon topography and data locations and hence is much smaller than the usual structured grids in standard, integral equation approaches. The method allows fast forward modelling to be achieved without explicitly forming the large, dense sensitivity matrix associated with the integral equation. The principal ocTree mesh can be divided into sub-domains to increase the efficiency of the forward problem. The benefit of not forming the sensitivities explicitly is that large problems can be run with limited computer resources.

REFERENCES

Ascher, U. M. and Haber, E., 2001, Grid refinement and scaling for distributed parameter estimation problems: Inverse Problems, 17, 517-590.

Bhattacharyya, B. K., 1964, Magnetic anomalies due to prism-shaped bodies with arbitrary magnetizations: Geophysics, 29, 517-531.

Cordell, L., 1992, A scattered equivalent-source method for interpolation and gridding of potential field data in three dimensions: Geophysics, 57, 629-636.

Haber, E., Heldmann, S., and Ascher, U., 2007, Adaptive finite volume method for distributed non-smooth parameter identification: Inverse problems, 23, 1659-1676.

Lelièvre, P. G. and Oldenburg, D. W., 2006, Magnetic forward modelling and inversion for high susceptibility: Geophysical Journal International, 166, 76-90.

Li, Y., and Oldenburg, D. W., 2000, Joint inversion of surface and three-component borehole magnetic data: Geophysics, 65, 540-552.

Li, Y., and Oldenburg, D. W., 2003, Fast inversion of large-scale magnetic data using wavelet transforms and a logarithmic barrier method: Geophysics Journal International, 152, 251-265.

Li, Y., and Oldenburg, D. W., 2010, Rapid construction of equivalent sources using wavelets: Geophysics, 75, L51-L59.

Mareschal, J. C., 1985, Inversion of potential field data in Fourier tranform domain: Geophysics, 50, 685-691.

Phillips, N., Nguyen, T.N.H., and Thomson, V., 2009, QUEST Project: 3D inversion modelling, integration, and visualization of airborne gravity, magnetic, and electromagnetic data, BC, Canada; Geoscience BC, Report 2009-15, 79 p.

Pilkington, M., 1997, 3-D magnetic imaging using conjugate gradients: Geophysics, 62, 1132-1142.

Vogel, C. R., 2002, Computation Methods for Inverse Problems (Frontiers in Applied Mathematics): Society for Industrial Mathematics.